Revista de Chimie
https://revistadechimie.ro
https://doi.org/10.37358/Rev.Chim.1949

Low-temperature Synthesis of Carbon Nanofibers/graphite Felt Composites Under Contactless Induction Heating

CUONG DUONG-VIET[1]*, LAI TRUONG-PHUOC[1], THIERRY ROMERO[1], JEAN-MARIO NHUT[1], LAM NGUYEN-DINH[2], LOÏC VIDAL[3], CUONG PHAM-HUU[1]*

[1]Institute of Chemistry and Processes for Energy, Environmental and Health (ICPEES), UMR 7515 of the CNRS-University of Strasbourg, 25 Rue Becquerel, 67087, Strasbourg Cedex 02, France
[2]The University of Da-Nang, University of Science and Technology, 54, Nguyen Luong Bang, Da-Nang, Vietnam
[3]Institute of Materials Science of Mulhouse, IS2M, UMR 7361, Université de Haute-Alsace, CNRS, 15, Rue Jean Starcky - BP 2488, 68057, Mulhouse, France

***Abstract**: In this report induction heating was used for the catalytic chemical vapor decomposition synthesis of carbon nanofibers (CNFs) on Ni-based catalyst. The CNFs were produced with a high yield at a relatively low temperature compared to that observed for conventional heating through convection and conduction. The process also occurred in the absence of secondary toxic organic compounds, formed through side reaction in the high temperature gas-phase or through decomposition on the hot wall of reactor as encountered with traditional Joule heating mode. The improved CNFs yield under induction heating was attributed to the high reaction temperature control thanks to the high temperature regulation rate provided by the induction heating coil. The local heating of the nickel nanoparticles by the electromagnetic field could also contribute to the improvement of the CNFs yield. The results obtained indicate that inductive heating mode could be of great interest for improving the heat transfer in catalytic processes and also to reduce the problem of gradient temperature occurring inside the catalyst bed during the operating of highly exothermic or endothermic processes. It is expected that such electricity-driven heating mode could have contributed in an efficient way toward the electrification of different catalytic processes in order to reduce the associated carbon footprint.*

***Keywords:** induction heating, chemical vapor decomposition, carbon nanofibers, catalysis, process electrification*

1. Introduction

Carbon nanomaterials, carbon nanotubes and nanofibers, have received an ever increasing scientific and industrial interest since the last decades for being used in several potential applications [1-6]. The nanoscopic dimension of the CNFs provides high accessible and low diffusion path for the reactant towards the active sites which contributes to an improvement of the overall catalytic performance. Carbon nanotubes (CNTs) display a tubular structure which could provide a nanometric confinement media for metal nanoparticles with different catalytic properties [7]. However, sintering phenomenon of metal nanoparticles seems to be easier on CNTs due to the weak interaction between the metal nanoparticles and the low reactivity graphite basal plane present on the surface of the CNT. Such interaction could be improved by doping the CNT with heteroelements such as nitrogen using an appropriate nitrogen source [8-11]. Carbon nanofibers (CNFs) with an exclusive presence of graphite prismatic planes which display higher interaction with the deposited metal nanoparticles compared to their counterpart CNTs have received an increasing scientific interest as support for heterogeneous catalysis field [12-17]. Such strong interaction, without a need for doping the material with foreign heteroelements and thus, a more simplify synthesis process, leads to a high metal nanoparticles dispersion which significantly improves the overall catalytic performance [18-22]. Sanz-Navarro et al. [20] have reported that the strong interaction between the prismatic planes and the deposited platinum nanoparticles leads to the restructuration of the metal particles and induces the appearance of strain in the Pt-Pt bond. Similar results about the role of prismatic planes to stabilize the decorated metal nano-

**email: duongviet@unistra.fr, cuong.pham-huu@unistra.fr*

particles have also been reported in other works [17, 23, 24].

For catalytic applications, and especially for the gas-phase processes, the direct use of CNF as catalyst support is hampered due either to the problems linked with the nanoscopic dimension of the material which induces high pressure drop across the catalyst bed and also for transport and handling. Numerous reports have been devoted to the synthesis of CNFs composites with controlled macroscopic shaping for heterogeneous catalysis applications [25-30]. The advantages of hierarchical structured supports made of CNFs are numerous: (i) high effective surface area and short diffusion path for reactants diffusion in and for intermediate product diffusion out, (ii) low pressure drop for fixed-bed catalyst bed even when operated under high gaseous velocities, (iii) lack of ink-bottled pores which could hinder the accessibility to the active phase. In addition, when the CNFs are supported on a conductive carbon host matrix the overall thermal conductivity of the composites is also significantly improved which contributes to the reduction of local hot spots within the catalyst matrix.

For CVD process the inductive heating displays several advantages in terms of the rapidity to direct the input energy to the target, the high selectivity of the heating area and the lack of any thermal induced secondary reactions on the reactor wall [31, 32]. Indeed, in the case of inductive heating the reactor walls, which is constituted generally by quartz, is transparent with respect to the induction and remains at much lower temperature than the growth catalyst which is actively coupled and thus, prevents the occurrence of secondary reactions leading to the formation of toxic organic compounds from the carbon source on the reactor wall as generally observed under traditional Joule heating. The inductive heating provides a rapid temperature to the catalyst thanks to the direct heating of the carbon-based support through eddy current contrary to the conventional Joule effect where a large part of the heat delivered is wasted through heat dissipation by convection or thermal radiation within the synthesis setup [33, 34]. According to the advantages listed above the energy transfer by inductive heating is more effective compared to other heating modes [35, 36]. Inductive heating has been efficiently used for the CVD synthesis of carbon nanotubes and graphene [37-41]. The rapid heating/cooling allows the precise control of the growth/quenching of the process which leads to materials with better quality. Inductive heating was also efficiently used as heating mean for numerous catalytic processes where heat transfer represents the main bottleneck to the processes [42-53]. Inductive heating can also be efficiently used for local deposition of one-dimensional materials on MEMS [54, 55].

The aim of the present work is to report on the use of inductive heating setup for the CVD synthesis of hierarchical carbon nanofibers (CNF) decorated carbon felt composites with nickel as growth catalyst and ethane as carbon source. The inductive heating allows the rapid synthesis of the hierarchical CNFs/GF composites at extremely low reaction temperature compared to that of the conventional Joule heating which could be attributed to a better heat targeting and regulation. The cold wall operating mode allows one to avoid secondary reactions leading to the formation of toxic high weight organic compounds, either through thermal decomposition of the intermediates on the reactor wall or directly as homogeneous combination reaction in the gas-phase medium, as encountered with traditional CCVD process carried out under Joule heating mode. The difference in terms of synthesis temperature, CNF yield, and specific surface area between inductive and conventional Joule heating will be discussed. Inductive heating also allows one to produce CNF with smaller diameter compared to Joule heating under similar reaction temperature.

2. Materials and methods

2.1. Support and catalyst

The commercial filamentous GF, ex-polyacrinonitrile (PAN), with a dimension of 1 x 3 m^2 (thickness of 6 mm) was supplied by Carbone Lorraine (MERSEN, La Défense, France). The as-received GF was shaped in the form of disks (Ø × thickness of 26 × 12 mm) for the experiment. The GFs displays a relatively low specific surface area, 4 ± 2 m^2/g measured by means of N_2 adsorption, which is mostly linked with its geometric surface area and is in good agreement with the lack of internal porosity of the material. The corresponding SEM micrographs of the pristine GF substrate with different magnification

are presented in Figure 1 showing the well separate microfilaments of the GF and their smooth surface and absence of internal porosity confirming the low SSA of the sample.

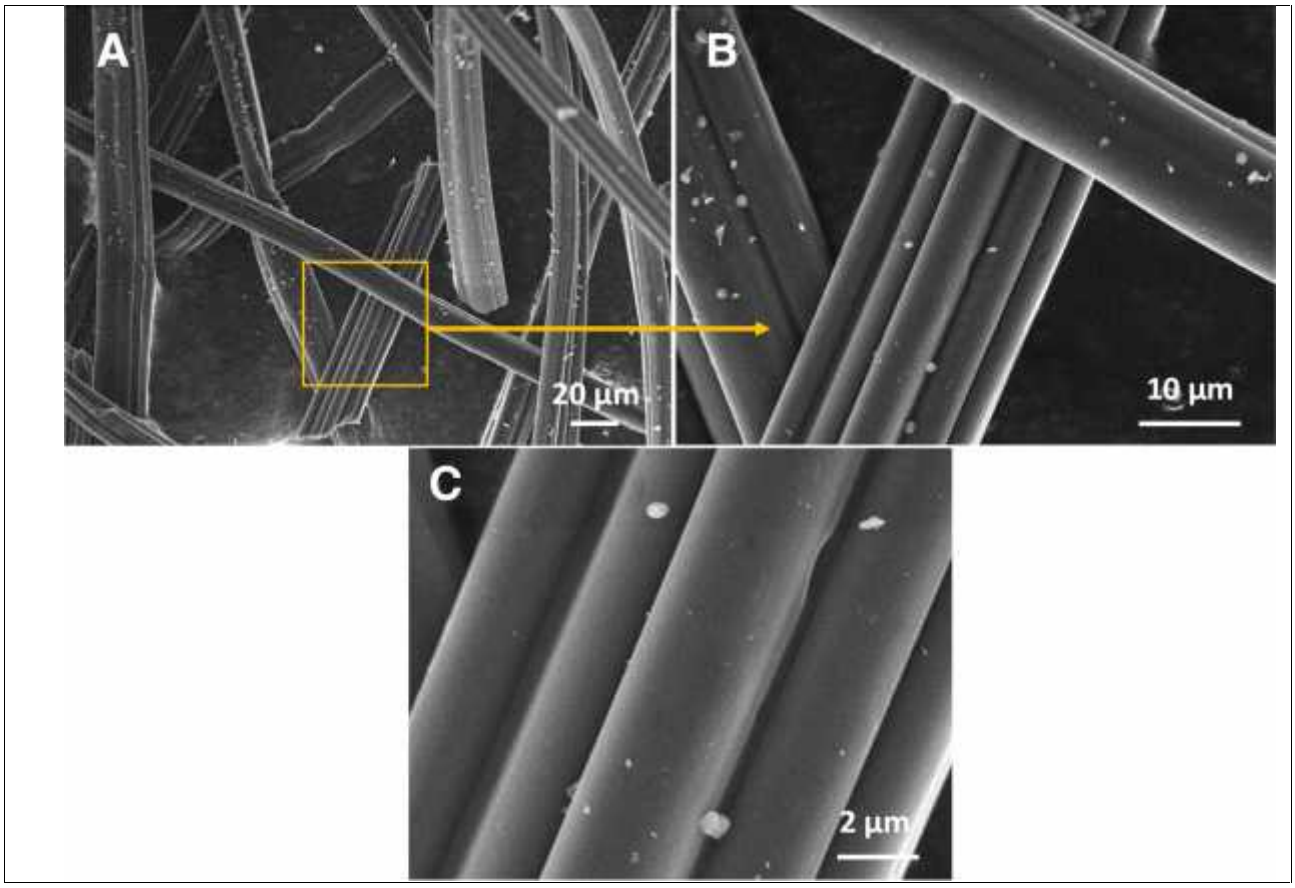

Figure 1. (A, B) SEM micrographs of the pristine graphite felt with a highly entangled morphology and smooth surface. (C) High resolution SEM micrograph showing the lack of internal porosity inside the filament

The catalyst was consisted by a nickel nanoparticles dispersed on the carbon felt with a theoretical nickel loading of 2 wt. %. The nickel was deposited via an incipient wetness impregnation method using a nickel nitrate aqueous solution as salt precursor ($Ni(NO_3)_2.6H_2O$, Fluka). The impregnated solid was oven dried at 110°C for 2 h to gently evaporate the solvent and calcined in air at 350°C for 2 h in order to decompose the nickel nitrate into its corresponding oxide. Before the growth process the catalyst was further reduced in-situ under hydrogen flow (60 mL. min^{-1}) at 350°C for 2 h.

3.2. Carbon nanofibers growth process

The carbon nanofibers (CNFs) decorated carbon felt composites were synthesized by Chemical Vapor Deposition (CVD) method using both inductive heating and conventional Joule heating modes. The GF piece (diameter, 26 mm, thickness, 12 mm) was placed inside a quartz reactor (inner diameter, 26 mm, external diameter, 30 mm, length, 400 mm). The reactor was placed either inside an induction coil (without external insulation) or inside a Joule heated electrical tubular oven with insulation plugs on both ends of the oven.

The direct IH mode was operated using an induction heating system (EASYHEAT LI 8310, Ambrell Ltd.) equipped with laser pyrometer (OPTCTL3MH1CF2, Optris, Germany). The induction coil is constituted by a spiral 6-turn copper coil (length = 1.05 m, pure coil resistance = 2.066 x 10-3 Ω), cooled by means of an external chiller with recirculated water/glycerol (10%) mixture operated with a nominal power of 10 kW and a frequency of 270 kHz. For the experiment, a quartz reactor (ID = 10 mm, length

= 400 mm, without any insulation) containing the catalyst, localized between two quartz wool plugs, was housed inside the induction coil and the temperature was monitored by a PID system (Proportional Integral Derivative controller, Eurotherm model 3504) connected to a laser pyrometer (Optris, ∅ laser beam: 500 µm, power < 1 mW, located at ca. 30 cm from the reactor) focused on the catalyst bed (GF susceptor) and working in the 150-1000°C temperature range with an accuracy of ± 1°C. The GF disk containing the growth catalyst was heated up through the eddy current from the induction coil No thermocouple was used to measure the reaction temperature due to it high coupling efficiency with the induction coil.

The reactor temperature was raised from 350°C to the desired temperature within few minute (heating rate of 50°C. min^{-1}). At the desired temperature the H_2 flow was replaced by a mixture of ethane and hydrogen (total flow rate, 20 and 100 mL min^{-1}) and the synthesis was lasted at different synthesis temperature for 2 h. Hydrogen was used as co-reactant as it could help to prevent carbon layer encapsulation of the growth catalyst [56]. Hydrogen could also have influenced the surface restructuration of the growth catalyst which in turn, modifies the structure of the deposited carbon nanofilaments [57]. After the synthesis the reactor was cooled down from the reaction temperature, i.e. 620-700 °C, to < 150°C within few minutes through rapid solid quenching and heat exchange with the surrounding atmosphere medium, and the reactant mixture flow was replaced by an argon flow and the product was discharged from the reactor at room temperature. At low temperature, < 150°C, the natural cooling through convection with the external medium remains the limiting step. However, at such low temperature no reaction is expected to occur.

For comparison the same synthesis was also evaluated under indirect Joule heating using an electric oven (ERALY Co., $\varnothing_{OD}$ = 200 mm, $\varnothing_{ID}$ = 55 mm, length = 300 mm, I_{max} = 8.6 A, T_{max} = 1100°C). The reactor was housed inside a tubular electrical oven and both ends were insulated with quartz wool plugs. The catalyst was reduced under the same reaction conditions as those used for the IH mode and the reaction was evaluated under the same conditions as described above. The temperature was measured by two thermocouples, one inserted inside the oven and one is attached to the external wall of the reactor. The reaction temperature was controlled by the thermocouple located inside the oven. It is worthy to note that for the Joule heating the increase of the reaction temperature takes longer time due to the high thermal inertia of the electrical oven. In the Joule heating mode, the carbon felt containing nickel oxide precursor was reduced in situ under H_2 flow at 350°C (heating rate of 20°C. min^{-1}) for 2 h. Then, the reactor temperature was raised from 350°C to the reaction temperature (heating rate of 30°C min^{-1}) and the H_2 flow was replaced by a mixture of ethane and hydrogen (total flow rate, 20 and 100mL min^{-1}) and the synthesis was lasted at the set temperature for 2 h. The reactor was cooled down under the reactant mixture flow down to 400°C and then, the reactant mixture flow was replaced by an argon flow and the product was discharged from the reactor at room temperature. Details of the synthesis can be found in previous reports [58]. As stated above, the high thermal inertia of the electrical oven cannot allow the rapid quenching of the reaction temperature, similarly to that used for the IH mode, and thus, the temperature decrease takes much longer time, i.e. 2 h instead of few minutes, to be under < 150°C.

3.4. Characterization techniques

The scanning electron microscopy (SEM) was carried out on a ZEISS 2600F with a resolution of 5 nm. The sample was deposited onto a double face graphite tape in order to avoid charging effect during the analysis.

The TEM analysis was carried out on a JEOL ARM- 200F working at 200 kV accelerated voltage, equipped with a probe corrector for spherical aberrations, and a point-to-point resolution of 0.2 nm. The sample was dispersed by ultrasounds in an ethanol solution for 5 min and a drop of the solution was deposited on a copper covered with a holey carbon membrane for observation.

The specific surface area of the support and the catalyst, after reduction, were determined in a Micromeritics sorptometer. The sample was outgassed at 250°C under vacuum for 8 h in order to desorb

moisture and adsorbed species on its surface. Physisorption measurements were carried out using N_2 as adsorbent at liquid N_2 temperature at relative pressures between 0.06 and 0.99.

The Raman spectra were recorded using LabRAM ARAMIS Horiba Raman spectrometer equipment. Spectra were recorded over the range of 500 - 4000 cm^{-1} at the laser excitation wavelength of 532 nm. The sample was deposited on glass substrate by deep-coating of its suspension and carefully dried before measurement.

X-ray photoelectron spectroscopy (XPS) measurements were carried out on a Thermo Fisher ESCALAB 250Xi spectrometer equipped with monochromatic Al Kα (hυ = 1486.6 eV, 15 kV, 10.8 mA). The binding energies were calibrated on the carbon C1s peak at BE = 284.6 eV (accuracy within ± 0.1 eV).

Thermal gravimetric analysis (TGA) was realized on a TGA Q5000 instrument with a heating rate of 10°C/min under air atmosphere. The weight of the sample was keep at around 10 mg in order to avoid diffusion problems during the analysis.

3. Results and discussions

3.1. Ni@GF characteristics

The Ni@GF catalyst, after calcination and reduction under hydrogen at 350°C for 1 h under IH mode, was characterized by TEM and the representative TEM micrographs are presented in Figure 2. Low magnification TEM and STEM-HAADF micrographs (Figure 2 A and C) clearly show the relatively high dispersion of the Ni NPs across the GF surface despite the low specific surface area of the support. Such dispersion could be attributed to the presence of some surface defects as such or functionalized with oxygenated groups on the GF which play the role of anchorage sites for hosting the Ni NPs [59-61]. The average Ni particle size measured by statistical TEM is in the following order: 30 ± 10 nm for the IH reduction and 50 ± 10 nm for the JH reduction step (not shown). EDX and STEM-EELS analysis confirms the evenly repartition of the Ni NPs on the GF surface (Figure 2 B and D).

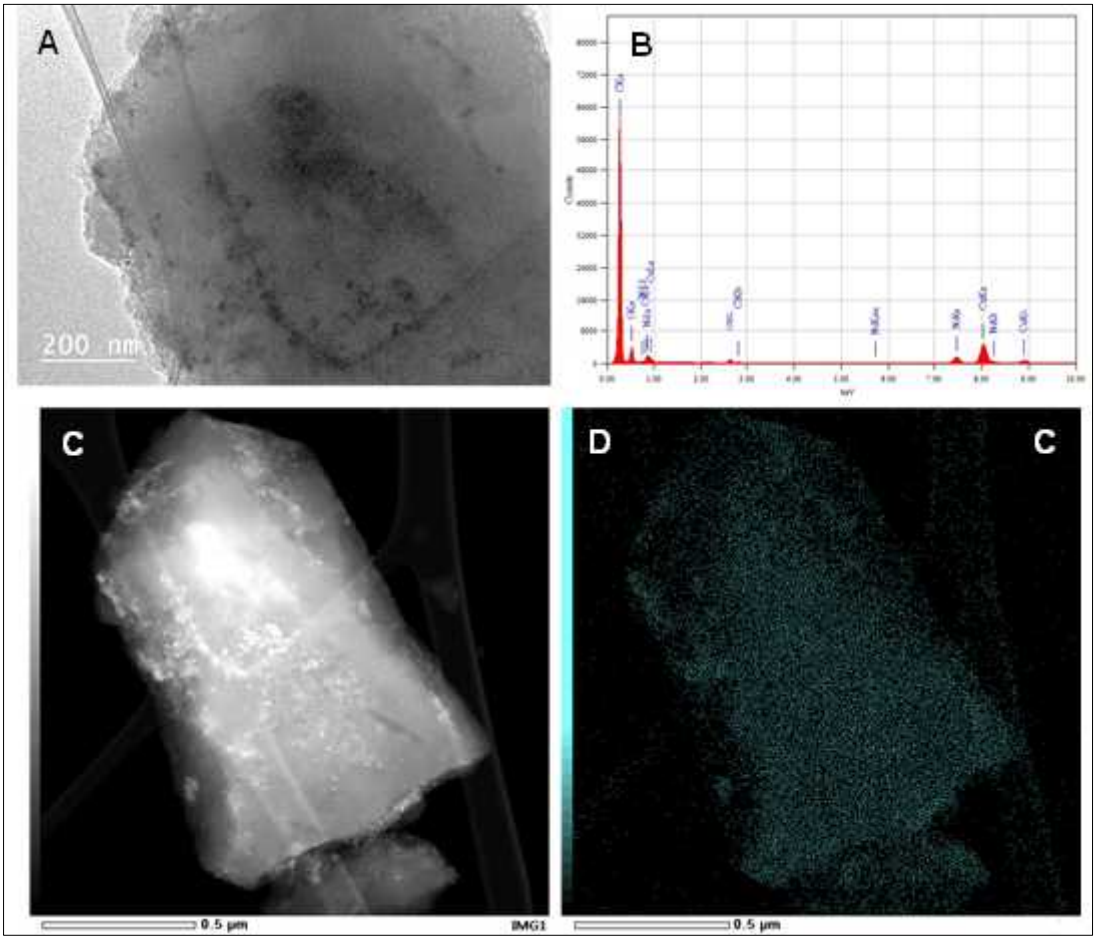

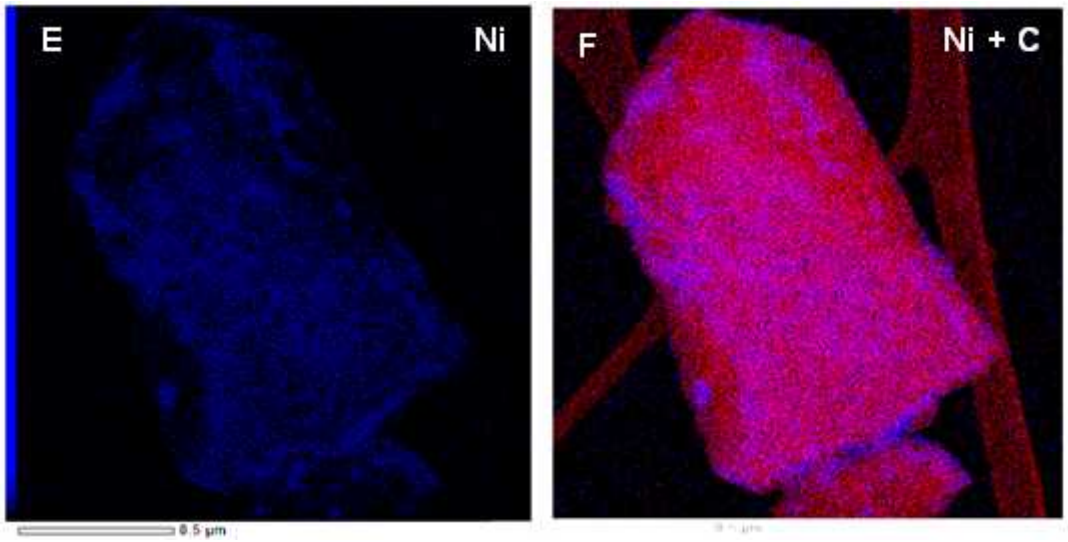

Figure 2. (A) Low magnification TEM micrograph showing the evenly dispersion of Ni NPs (indicated by arrows) on the GF felt after a reduction step at 350°C under IH mode and (B) the corresponding EDX spectrum of the sample. (C) STEM-HAADF micrograph of the Ni/GF catalyst after thermal treatment. (D-F) Corresponding STEM-EELS elemental mapping of the sample in C showing the relatively high dispersion of the Ni NPs across the GF surface

3.2. Inductive heating vs Joule heating for CNF growth

The carbon nanofibers (CNFs) yield and specific surface area (SSA), as a function of the synthesis temperature for a fixed duration of 2 h and under a mixture of C_2H_6:H_2 of 50 mL: 75 mL. min^{-1}, using inductive heating (IH) and Joule heating (JH), are presented in Figure 3A. The CNFs yield increases proportionally with the reaction temperature for both heating modes which is in good agreement with the CVD process on nickel growth active sites [62]. The CNF yield is always higher regardless the synthesis temperature under IH compared to JH as highlighted in Figure 3A. Such difference could be attributed to the fact that under inductive heating the heat is directly generated within the catalyst, i.e. Ni@GF, and thus, no heat lost was encountered as usually occur with traditional Joule heating. Indeed, it is expected that for Joule heating the real catalyst surface temperature is underestimated due to large heat lost through radiation and gas exchange while the low inertia of the oven is unable to compensate and to maintain the heat for the reaction within the catalyst bed. In addition, the fast temperature regulation of the IH mode allows one to keep the catalyst temperature as close as possible to the set temperature despite the high endothermic character of the CVD process. Such on-spot temperature regulation could significantly have contributed to the improvement of the CVD process operated under IH compared to that operated under JH mode.

The results also indicate that CNF growth has already been initiated at reaction temperature as low as 620°C under IH mode (Figure 3A (left)). It is worthy to note that with conventional Joule heating almost no CNF growth process was observed at such low synthesis temperature (Figure 3A (right)). The ability of IH to initiate catalytic processes at much lower temperature than JH has already been observed by other groups [47, 63-66]. Such results could be explained by the fact that the high heating rate of the IH and the lack of thermal inertia allow one to maintain the reaction temperature as close as to the theoretical one which is not the case for the JH mode due to high inertia in temperature regulation as discussed above. In addition, for carbon material the heat provided by the IH is mostly issued from eddy current and is also mostly located on the material surface [50], where the reactions take place, and thus, strongly contributes to the improvement of the overall catalytic process efficiency. In addition, a second parameter which could be considered is the influence of the magnetic field on the Ni active phase. Indeed, the superior CVD activity under direct IH mode could also be attributed in part to the higher

surface temperature of local Ni NPs on the support through magnetic interactions. Such local high temperature can operate without changing the macroscopic temperature of the whole catalyst bed as reported previously by Chaudret and co-workers during the oxygen evolution reaction and hydro-deoxygenation processes [47]. In fact, the authors have attributed the high catalytic performance by an over-heating of the surface of the nano-catalyst, i.e. FeNi nanoparticle, which induces local high temperatures well above the boiling point of the solvent in which the reaction takes place. The heat generated on such local high temperature was rapidly dissipated into the whole catalyst matrix and the reactions were completed despite the relatively mild reaction conditions used. Similar results have also been recently reported by Wu et al. [53] on Ni supported on CaO-C catalyst for the production of hydrogen from biomass steam gasification process.

The SEM micrographs of the CNF@GF composites, with different magnifications, obtained after the CVD at 700°C for 2 h under the two heating modes are presented in Figure 3B to E. Under IH the CNF diameter is much smaller compared to that obtained under indirect JH (Figure 3E vs 3C). The difference in terms of CNFs diameter observed between the CNFs/GF composites synthesized by inductive and Joule heating could be explained by the difference of the heating mode. In the inductive heating the temperature of the catalyst, Ni/GF, was rapidly ramped up as soon as the heating start, and thus, sintering of the nickel growth catalyst could be significantly reduced before the CNFs growth process is initiated. On the contrary, for conventional Joule heating the time to reach the desired synthesis temperature is much longer and thus, during such period, thermal sintering of the nickel nanoparticles on the GF could occur, leading to bigger nickel particles when the catalyst reached the growth temperature. Literature reports have unanimously on the direct relationship between the carbon nanofibers or nanotubes diameter and the metal particle size acting as growth catalyst regardless the growth mechanism, i.e. tip- or base-growth [67, 68]. According to the literature reports, such difference in terms of nickel particles for the subsequence growth of the CNFs is expected to be at the origin of the large difference in terms of the CNFs diameter between the two heating modes. The catalyst particle size has also a significant influence on the CNFs growth rate and thus, the CNFs yield. It has been reported that the carbon growth rate is faster on small catalyst particle compared to the bigger ones which could be attributed to the fast diffusion of dissociated carbon through the small growth metal particle. In addition, it is worthy to note that under JH the CNFs were in a grumbled morphology wrapping around the GF substrate whereas under IH, the CNFs seem to growth in a perpendicular direction with respect to the axis of the GF substrate. Such phenomenon could be attributed to some influence of the magnetic field on the Ni growth center and orientation. Work will be carried out to get more insight about such phenomenon.

Digital photos of the reactor after the CVD synthesis by inductive or Joule heating carried out at 700°C, are presented in Figure 3 Fi and ii. The results clearly indicate the absence of thermal de-composition organic compounds on the reactor wall with inductive heating as the wall remains transparent after the synthesis. Such results are expected taken into account that only the catalyst is keep at the reaction temperature while the reactor wall and the gas phase leaving the catalytic zone remain at much lower temperature which prevent thermal decomposition of the intermediate products to make carbonaceous residues similarly to the results reported by Santamaria and co-workers under microwave process [69]. On the other hand, the reactor wall with Joule heating displays the presence of dark brown compounds (Figure 3Fi) which are originated from non-catalytic thermal decomposition of the carbon precursor or intermediate product through secondary reactions on the hot wall of the reactor. Such thermal decomposition is also at the origin of the formation of some amorphous carbon on the final material during the cooling process and also of the heavy hydrocarbon residues at the exit of the reactor which render the recycling of the reaction feed difficult. The effluent containing heavy hydrocarbons also needs to be treated before releasing it into atmosphere.

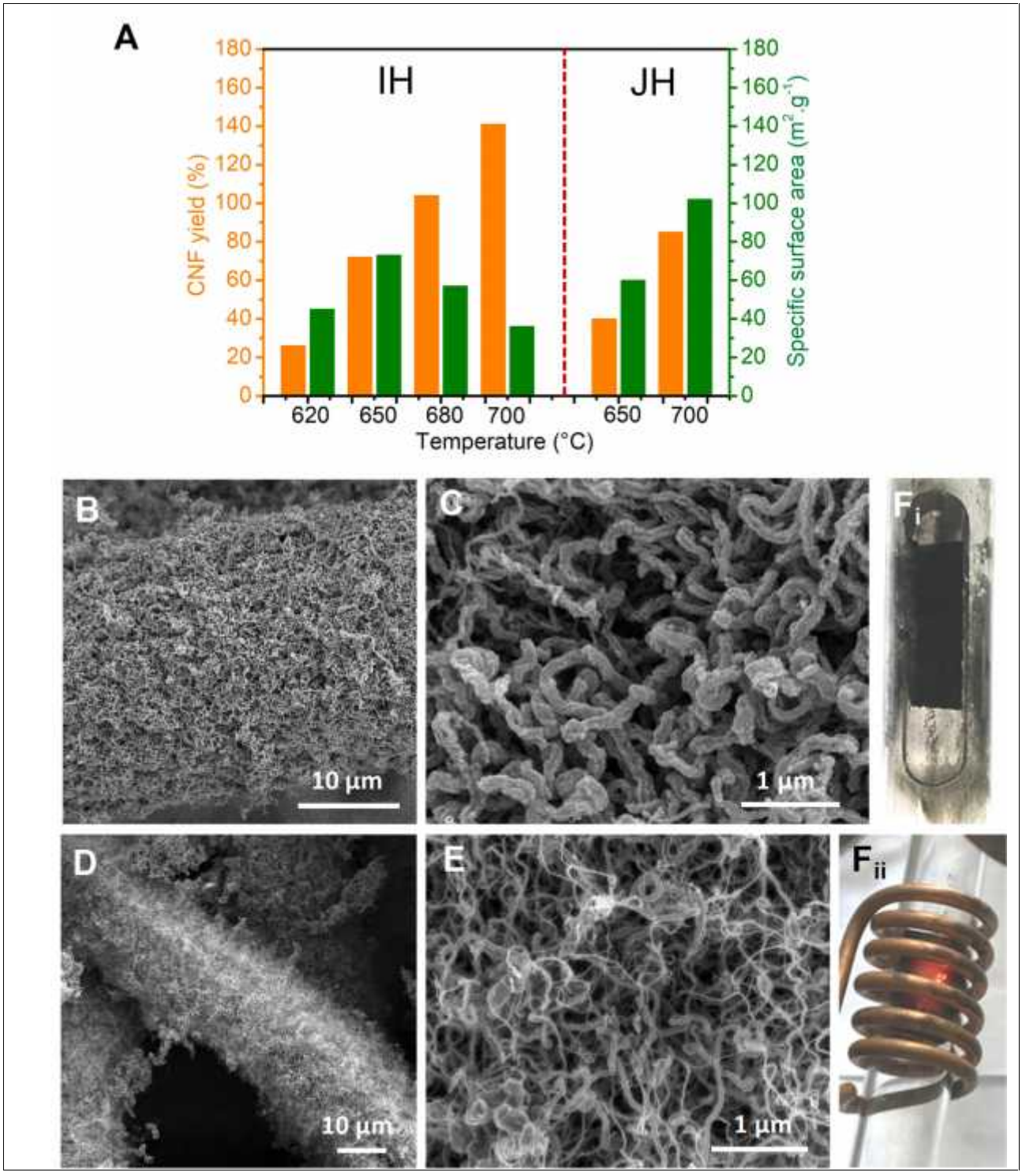

Figure 3. (A) Comparison for CNFs yield and SSA of the CNF@GF composites synthesized under inductive (IH, left side) and conventional Joule heating (JH, right side) on the Ni@GF catalyst as a function of the synthesis temperature with a duration of 2 h. At 620°C almost no CNFs growth was observed under JH mode. (B-E) Carbon nanofibers morphology obtained at 700°C during 2 h under conventional Joule (B, C) and induction (D, E) heating. (F_i-F_{ii}) Digital photos of the reactor wall after the CVD process using inductive and Joule heating at 700°C showing the complete absence of any carbon-based compounds on the reactor wall compared to that using Joule heating

The SEM micrographs of the CNF@CF composites synthesized at different temperatures and under IH mode are displayed in Figure 4. At the synthesis temperature of 620 and 650°C a homogeneous layer of CNFs was observed on the whole surface of the carbon microfilamentous (Figure 4A and B). However, at such low synthesis temperature the CNFs network is inhomogeneous and part of the GF remains uncovered as shown in Figure 4A and B. At higher synthesis temperature, i.e. 680 and 700°C, the layer of CNFs becomes much dense with a crumbled morphology as shown in Figure 4E and H which could be at the origin of the low SSA. The low SSA of the composites synthesized at high temperature could be attributed to the fast growing of the CNFs leading to a CNFs layer with high apparent density which bonded together to form a structure with lower accessibility. It is also worthy to note that at synthesis temperature of 680 and 700°C, some carbon nanoparticles were also observed alongside with the CNFs network, and could be attributed to the fact that at higher synthesis temperature the hydrocarbon gets faster decomposition to form large amount of carbon species on the catalyst particles leading to the formation of such carbon nanoparticles. Such carbon nanoparticles would also contribute to the lowering of the final surface area of the composites. It is also worthy to note that under IH mode the diameter of the as-synthesized CNFs remains small compared to that observed under JH mode. Such phenomenon could be directly linked with the problem of sintering of the metal growth catalyst under the heating mode.

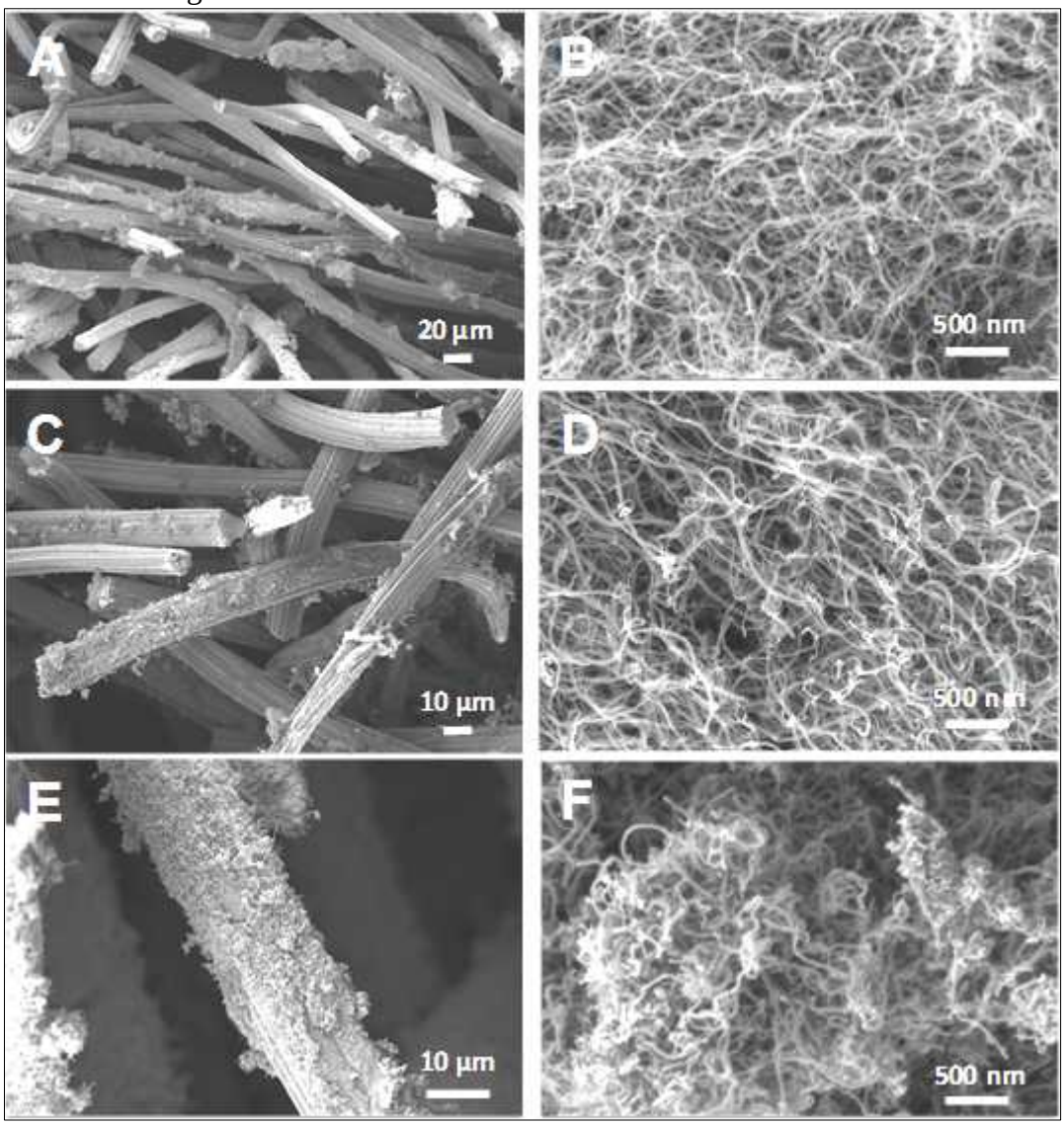

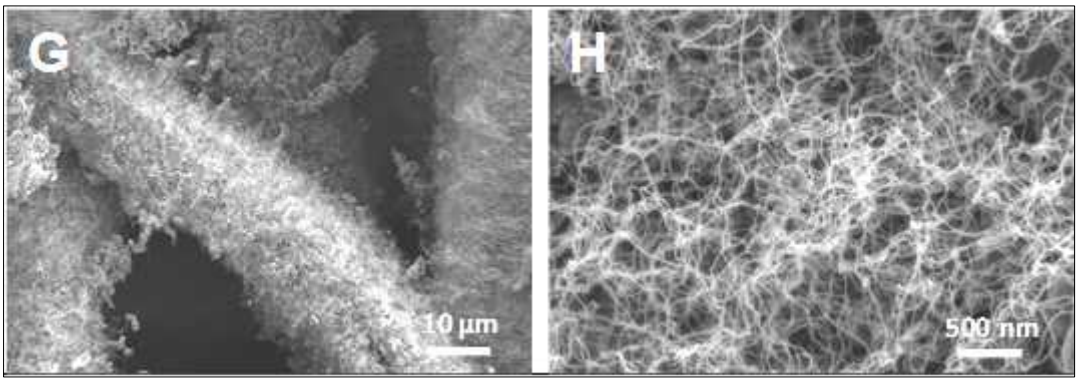

Figure 4. SEM micrographs showing the coverage and morphology of the CNF in the CNF@CF composites synthesized under inductive heating as a function of the reaction temperature with a mixture of C_2H_6:H_2 (50 mL:75 mL. min^{-1}) for 2 h. (A, B) 620°C, (C, D) 650°C, (E, F) 680°C, and (G, H) 700°C

SEM micrographs with medium resolution confirm the homogeneous diameter of the CNFs generated under IH mode (Figure 5). Such results could be explained by the relatively high Ni NPs dispersion on the growth catalyst according to the TEM results. In addition, the high heating rate applied to the catalyst under IH mode could also prevents the sintering of the metal particles compared to the JH mode where the set temperature was reached with longer time which could cause some sintering of the growth catalyst as discussed above.

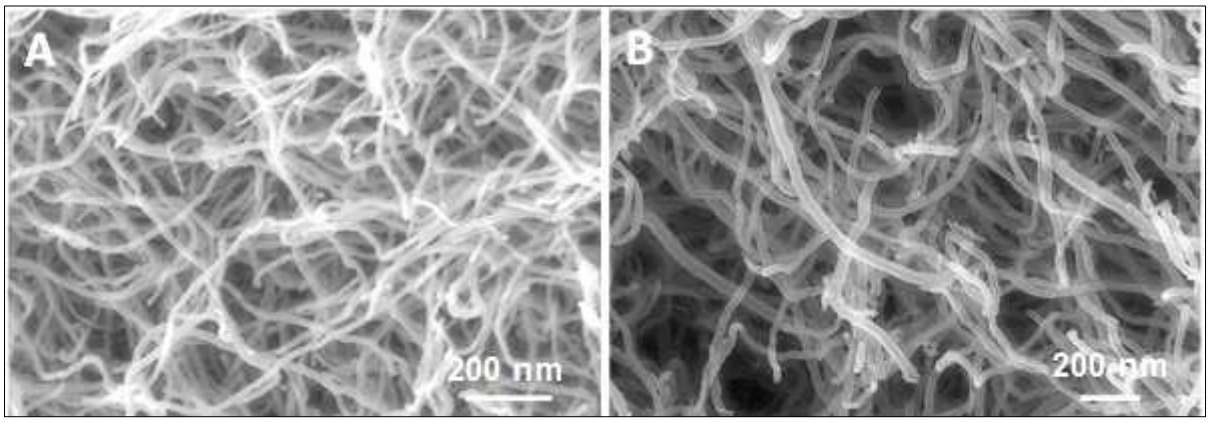

Figure 5. SEM micrographs of the CNFs synthesized at 620 and 650°C under direct IH mode showing the homogeneous distribution of the CNFs with relatively small diameter

The defective nature of the as-synthesized CNFs by inductive heating is investigated by means of the Raman spectroscopy and the results are presented in Figure 6. The I_D/I_G ratio of the composites increases with the CNFs loading which could be directly attributed to the generation of more defects inside the samples (Figure 6A). The carbon nanofibers growth from inductive heating is also more defective than the same growths from Joule heating according to the Raman results in Figure 6B. Such results could be explained by the growth rate of the CNFs according to the heating mode which induces different microstructures with various defects. In the report of Page et al. [70] it has been reported that the number of C_5, C_6 and C_7 rings created during the growth strongly depends on the carbon precursor decomposition rate. The fast decomposition rate leads to a fast growth of single-walled CNTs which also contains a higher number of defects. On the other hand, a slow decomposition rate allows the catalyst particle to reorganize and thus, large amount of C_6 ring is obtained leading to the formation of carbon nanotubes with lower defects.

XPS analysis indicated the presence of oxygenated functional groups on the surface of the as-synthesized CNF@GF composites upon air exposure at room-temperature (Figure 6C and D). Such oxygen decorated surface could be generated through exchange reaction between the H-bonding defect and oxygen in air and is expected to be localized on the defective sites of the carbon prismatic planes of the CNF. According to the XPS survey spectra in Figure 6C the relative amount of the oxygenated functional groups, i.e. O1s, in the CNF@GF composite, synthesized under IH mode, is much higher than that obtained in the one synthesized under JH mode. The O1s peak intensity of the CNF@GF composite from IH is as high as the one issued from the CVD using ethanol as carbon source where higher oxygen partial pressure was present.

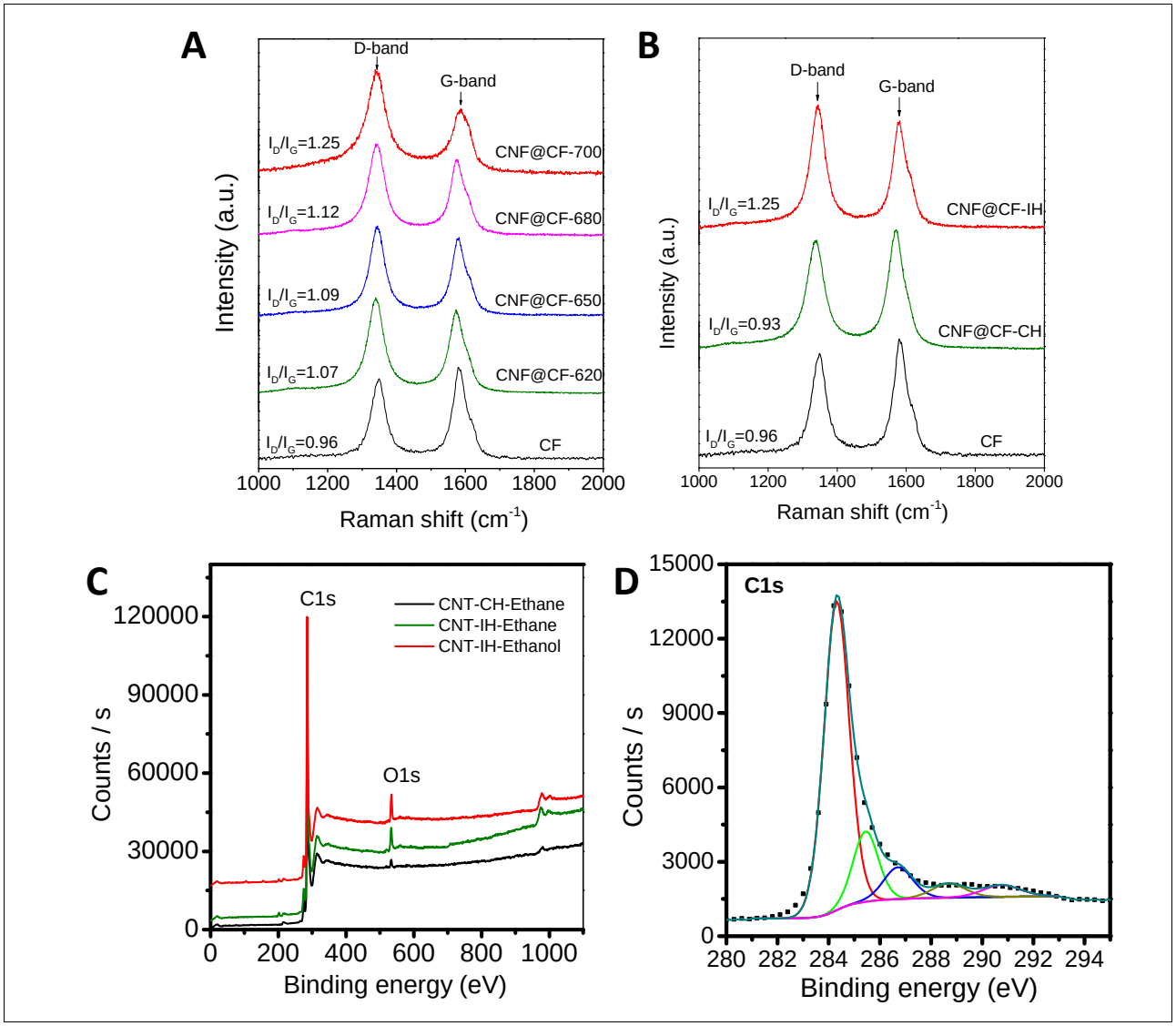

Figure 6. (A) Raman spectra of the CNFs/CF composites as a function of the synthesis temperature using inductive heating mode. The synthesis duration was kept for 2 h. (B) Raman spectra of the CNFs/CF composites obtained at 700°C and 2 h with inductive (IH) and conventional Joule heating (CF) modes. (C) XPS survey spectra of the CNF@GF composites synthesized with a mixture of C_2H_6/H_2 under IH and JH mode, and the one synthesized with ethanol under JH mode. (D) XPS C1s spectrum of the CNF@GF synthesized under IH showing the presence of C-O and C=O species

The CNF formed also leads to a significant improvement in terms of mechanical strength of the final composite compared to the pristine GF as evidenced by the digital photos in Figure 7A and B. The CNF@GF composite displays no apparent deformation under a weight of 100 g of load deposited on it

top whereas the pristine CF was already deformed under a weight twenty times lower. Such mechanical improvement is attributed to the generation of interconnected bridges, constituted by the high aspect ratio CNF, between the adjacent GF filamentous which link the composite structure as already been reported in our previous work [62] and also highlighted by the SEM micrographs in Figure 7C and D. It is expected that such mechanical improvement will be of great interest for the downstream applications, especially as support for heterogeneous catalysis where high mechanical strength is one of the prerequisites.

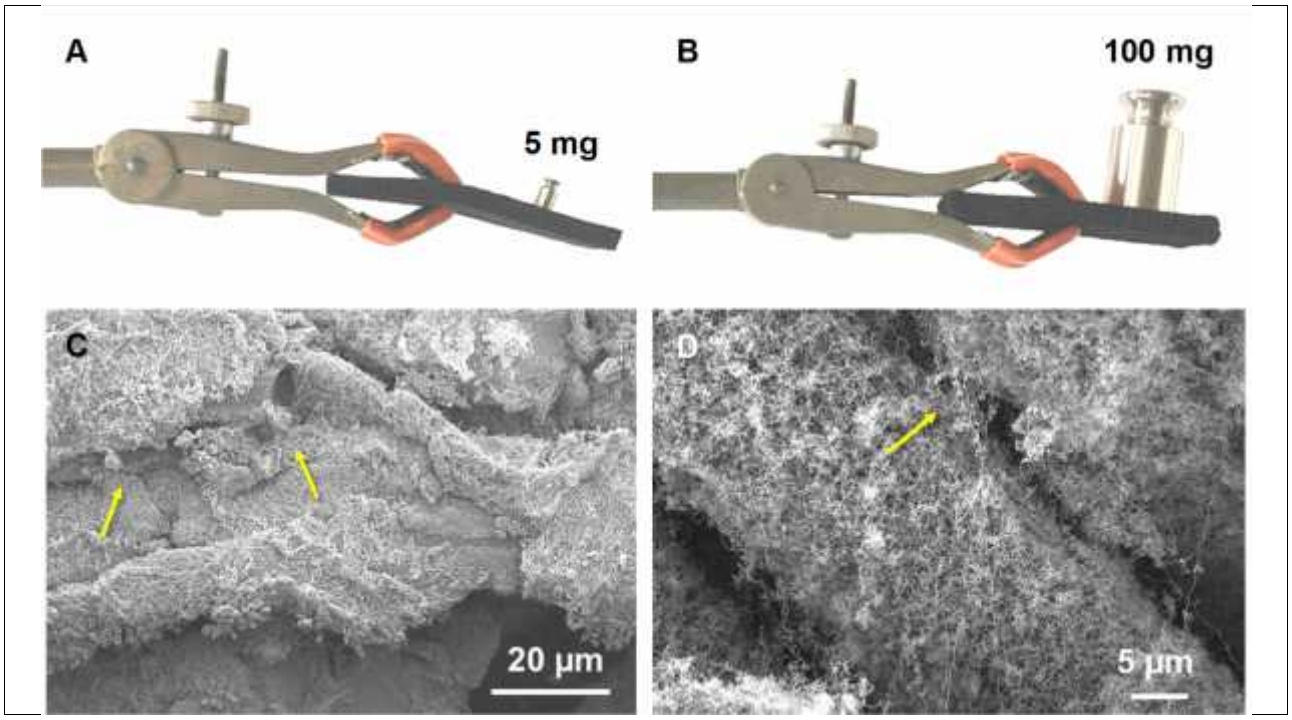

Figure 7. (A, B) Mechanical strength improvement between the pristine GF substrate and the final CNF@GF composite. (C, D) SEM micrographs of the bridging of the microfilaments by the CNF network (indicated by arrows)

3.2 Optimization growth of CNF under inductive heating

The results reported above have shown that the synthesis temperature of 650°C leads to the production of medium CNF yield along with the highest SSA. In this section the influence of the synthesis duration on the CNF yield and the composite SSA will be investigated at 650°C. First, the influence of the C_2H_6-to-H_2 volume ratio was investigated keeping the synthesis temperature at 650°C and duration of 2 h (Figure 8A). Increasing the C_2H_6-to-H_2 volume ratio leads to a significant increase of the CNF yield as higher carbon source was passed over the catalyst per time unit. However, when the C_2H_6-to-H_2 volume ratio was increased from 0.67 to 1, a decrease of the SSA was observed, i.e. 73 $m^2 . g^{-1}$ to 64 $m^2 . g^{-1}$. Such results could be attributed to the fact that at high C_2H_6 concentration the formation of some amorphous carbon with low SSA could occurred leading to a lower SSA for the final composite. The fast growth rate could also have led to a higher entanglement of the CNFs network with reduced accessibility and thus, contributing to a decrease of the SSA of the sample.

For the influence of the synthesis duration the C_2H_6-to-H_2 volume ratio of 0.67 was chosen. According to the results, the increase of the synthesis duration, keeping the synthesis temperature at 650°C, leads to a continuous increase of the CNFs yield and SSA of the composites (Figure 8B). The results clearly indicate that the loss of the SSA for the sample synthesized at 700°C observed in Figure 3A is mainly due to the change of the size of the growth catalyst on the CNFs properties at higher synthesis temperature and not directly linked to the CNF yield. It is expected that higher synthesis temperature could have led to the formation of CNF with bigger diameter, due to some sintering of the

nickel nanoparticles, as well as CNF with lower structural defect density which leads to a decrease of the overall SSA of the composites. For the CVD synthesis at 650°C under IH mode, the SSA of the final composite after 4 h reaction is amounted to ca. 130 m^2/g, taken into account the low SSA of the carbon felt support, i.e. 4 m^2. g^{-1}. Such value is among the highest SSA values for such hierarchical composites reported up until now in the literature [53]. It is expected that low temperature synthesis leads to the formation of CNF with homogeneous diameter (see SEM discussion below) along with relatively high structural defects which encounter for such high SSA. However, for a synthesis duration of 4 h the experimental CNF yield measured was slightly lower compared to the theoretical one determined by extrapolating the date obtained at 1, 2 and 3 h of synthesis, i.e. 116 wt.% instead of 128 wt.%. The results obtained allow one to tune in a relatively precise way the final characteristics of the CNF@GF composite, i.e. SSA or CNF yield, as a function of the downstream application.

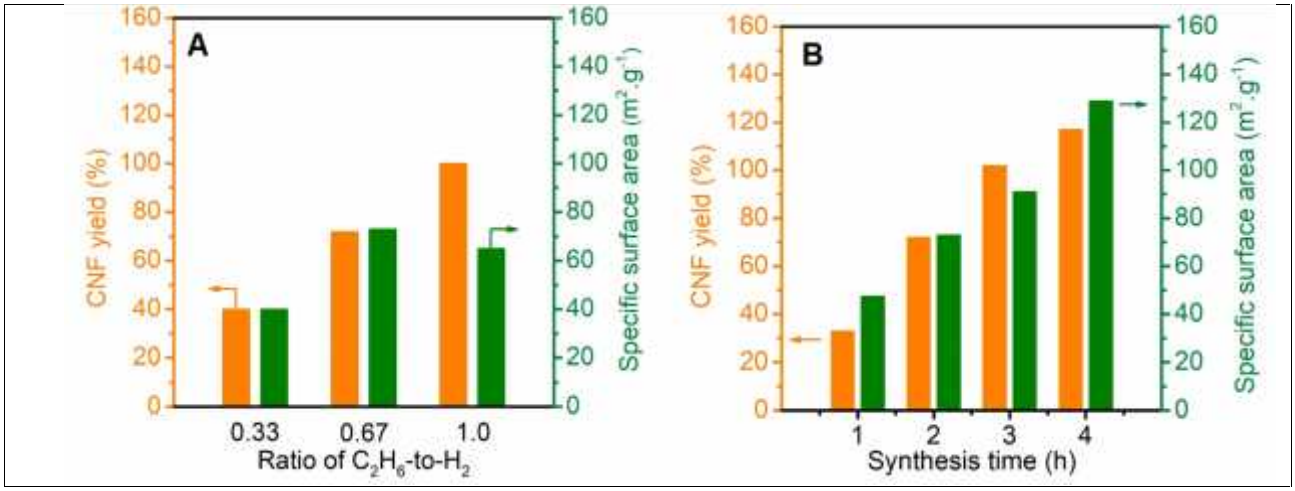

Figure 8. (A) CNF yield and associated SSA of the CNF@CF composites at 650°C for 2 h as a function of the C_2H_6 to H_2 ratio using inductive heating mode. (B) CNF yield and associated SSA of the CNF@CF composites at 650°C and with a C_2H_6-to-H_2 ratio of 0.67 as a function of the synthesis duration using inductive heating mode

TEM analysis was also used to characterize the microstructure of the as-synthesized CNF, at 650°C, and the results are displayed in Figure 9. The CNFs synthesized at 650°C display a relatively homogeneous diameter (as observed by SEM) and are consisted with a high proportion of small CNF with diameter centered between 50 to 80 nm (Figure 9A and B). Some larger CNF with diameter of ca. ≥ 100 nm are also observed among the sample which could be originated from some large Ni particles present in the catalyst.

These results confirm that CVD synthesis at 650°C favors the formation of small and high aspect ratio CNF with high SSA and exposure surface area which could be suitable for catalytic applications. Such results also highlight the efficiency of inductive heating to provide homogeneous and targeted heat to maintain the catalyst at almost isothermal temperature for the synthesis of CNFs at relatively low temperature compared to traditional Joule heating technique where the catalyst temperature maintaining remains problematic.

Statistical TEM analysis indicates the lack of Ni particle on the tip of the formed CNFs which confirms the high efficiency of the post-synthesis acid washing to remove the growth catalyst (Figure 9A and B). However, statistical TEM analysis reveals the presence of some nickel nanoparticles encapsulated within graphene layers which are not accessible to the acid and thus, remain inside the final composite (Figure 9C and D). Similar results have already been reported by several groups working in the field [71-73]. However, it is worthy to note that such residual growth catalyst is more often observed in the case of CNTs than CNFs. Such residual metal particles should not have any influence in the downstream catalytic applications as they are completely embedded under several graphene layers and

thus, remain inaccessible to the reactant. It is worthy to note that such encapsulated metal-carbon nanoparticles were observed more frequently in the sample synthesized at 700°C (not shown) and could be attributed to the high rate of carbon decomposition on the Ni surface which results in an encapsulation of the growth catalyst. Such TEM analysis thus confirms the fact that at high synthesis temperature high proportion of large diameter CNF and encapsulated metal-carbon particles are generated which display low SSA. High-resolution TEM micrograph (Figure 9D) also clearly shows the presence of graphitic planes arranged in a fishbone structure (indicated by arrows) along the growth axis of the CNF. It is also worthy to note that no amorphous carbon layer is observed on the topmost surface of the CNFs synthesized under IH mode whereas the CNFs synthesized under JH always display a thin layer of amorphous carbon on its topmost surface which is due to the secondary decomposition of the carbon source during the cooling step where amorphous carbon was preferentially formed atop of the CNFs surface. Such results could be explained by the high cooling rate of the CVD process under IH mode which reduces the deposition of amorphous carbon during the cooling step.

In order to verify if any small Ni NPs are present in the washed sample STEM-EELS analysis was also carried out on the sample. The spectra presented in Figure 9E to G confirm the high purity of the CNFs as no Ni NPs were detected in the analyzed sample, except some scarcely encapsulated metal particles as discussed above, and only carbon and oxygen (oxygenated functional groups decorated the prismatic planes of the CNF) elements were observed.

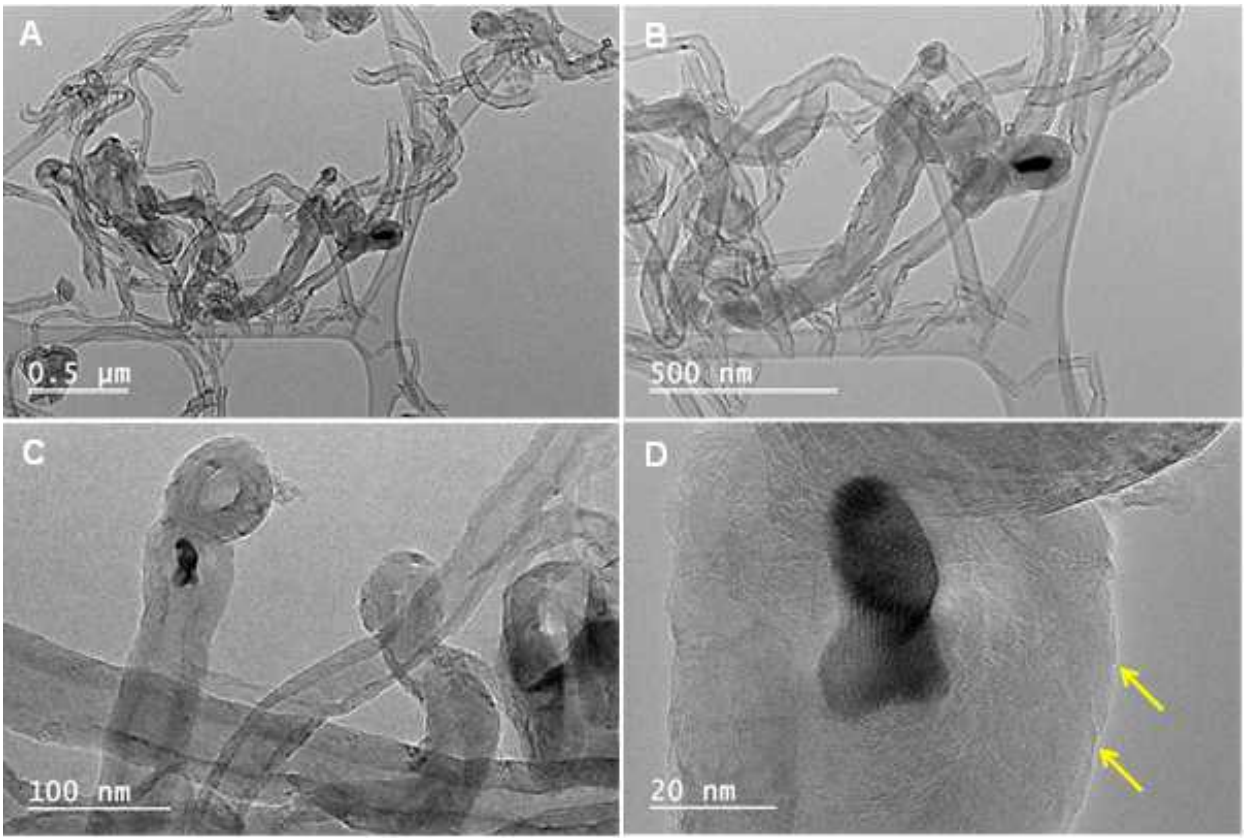

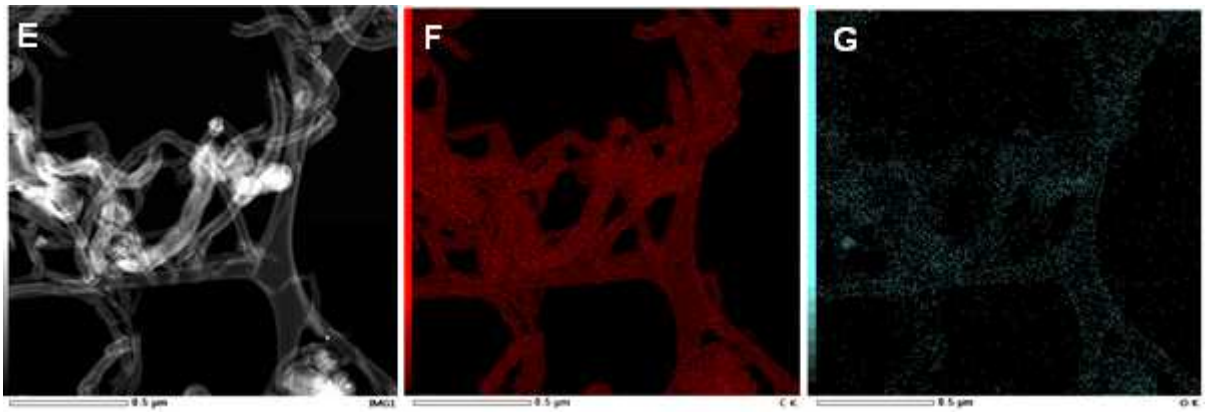

Figure 9. (A-C) TEM micrographs of the CNFs synthesized by inductive heating showing the tip growth mechanism with Ni particle located on the tip of the CNF. (D) High resolution TEM micrograph showing the fishbone-like structure of the CNF along the growth axis and the lack of amorphous carbon layer on the outer surface (indicated by arrows) (E-G) STEM-EELS micrographs showing the presence of carbon and oxygen elements.

4. Conclusions

In summary, inductive heating seems to be an appropriate technique for the CVD synthesis of carbon nanofibers with a high yield and with a complete absence of secondary toxic organic compounds, formed through side reaction in the high temperature gas-phase or through decomposition on the hot wall of reactor as encountered with traditional Joule heating mode. The improved CNFs yield was attributed to the reaction temperature accuracy, targeted exclusively to the catalyst, provided by inductive heating as no heat loss was expected compared to the Joule heating where a large part of the heat input has been lost due to heat transfer between the setup elements and also by the flue gas. Due to all the heat loss, and especially through the solid-gas phase exchange, and also to the high inertia of the electrical oven to compensate/maintain the reaction temperature, it is expected that the surface temperature of the catalyst heated by Joule heating mode is lower than that fixed by the oven which could explain the large difference in terms of CNF yield between the two heating mode. The local heating of the nickel nanoparticles by the electromagnetic field could also contribute to the production of the CNFs. The results obtained indicate that inductive heating mode could be of great interest for improving the heat transfer in catalytic processes and also to reduce the problem of gradient temperature occurring inside the catalyst bed during the operating of highly exothermic or endothermic processes. It is expected that such electricity-driven heating mode could have contributed in an efficient way toward the electrification of different catalytic processes in order to reduce the associated carbon footprint. Work is ongoing to evaluate the inductive heating mode in a highly exothermic or endothermic reaction where rapid heating/cooling rate could be useful for the temperature management inside the reactor and to avoid local hot/cold spot formation which could be detrimental for operating catalytic processes.

Acknowledgements: The authors would like to thank Dr. V. Papaefthimiou (ICPEES, UMR 7515) for performing the XPS analysis and helpful discussion. The SEM and Raman experiments were carried out at the facilities of the SEM (ICPEES-IPCMS) and Raman platforms (ICPEES). TEM experiments were carried out at the TEM platform of IS2M (UMR 7361) facilities.

References

1. D. S. SU, S. PERATHONER, G. CENTI, Nanocarbons for the development of advanced catalysts. Chem. Rev. 113, 5782-5816 (2013).
2. M. J. LEDOUX, C. PHAM-HUU, Carbon nanostructures for catalytic applications. Catal. Today 102-103, 50-57 (2005).

3. J.-P. TESSONNIER, D. S. SU, Recent progress on the growth mechanism of carbon nanotubes: A review. ChemSusChem 4, 824-847 (2011) and references herein.
4. V. SINGH, D. YOUNG, L. ZHAI, S. DAS, S. I. KHOMDAKER, S. SEAL, Graphene based materials: Past, present and future**.** Prog. Mater. Sci. 56, 1178 (2011).
5. Z. LIN, Z. ZENG, X. GUI, Z. TANG, M. ZOU, A. CAO, Carbon nanotubes sponges, aerogels, and hierarchical composites: synthesis, properties and energy applications. Adv. Energ. Mater. 1600554 (2016).
6. K. P. DE JONG, J. GEUS, Catal. Rev. Sci. Eng. 42, 481-510 (2000).
7. J.-M. NHUT, P. NGUYEN, C. PHAM-HUU, N. KELLER, M.-J. LEDOUX, Carbon nanotubes as nanosized reactor for the selective oxidation of H_2S into elemental sulfur, Catal. Today 91, 91-97 (2004).
8. K. GONG, F. DU, Z. XIA, M. DURSTOCK, L. DAI, Nitrogen-doped carbon nanotube arrays with high electrocatalytic activity for oxygen reduction, Science 323, 760-764 (2009).
9. J. AMADOU, K. CHIZARI, M. HOULLÉ, I. JANOWSKA, O. ERSEN, D. BÉGIN, C. PHAM-HUU, N-doped carbon nanotubes for liquid-phase C-C bond hydrogenation, Catal. Today 138, 1-2, 62-68 (2008).
10. L. M. MABENA, S. S. RAY, S. D. MHLAUGA, N J. COVILLE, Nitrogen-doped carbon nanotubes as a metal catalyst support, Appl. Nanosci. 1, 67-77 (2011).
11. G. TUCI, C. ZAFFERONI, A. ROSSIN, A. MILELLA, L. LUCONI, M. INNOCENTI, L. TRUONG-PHUOC, C. DUONG-VIET, C. PHAM-HUU, G. GIAMBASTIANI, Chemical functionalized carbon nanotubes with pyridine groups as easy tunable N-decorated nanomaterials for the oxygen reduction reaction in alkaline medium, Chem. Mater. 26, 3460-3470 (2014).
12. YADAV D., AMINI F., EHRMANN A., Recent advances in carbon nanofibers and their applications – A review, Eur. Poly. J. 138, 109963 (2020).
13. ZHANG B., KANG F. Y., TARASCON J.-M., KIM J.-K., Recent advances in electrospun carbon nanofibers and their application in electrochemical energy storage, Progress Mater. Sci. 76, 319-380 (2016).
14. RUIZ-CORNEJO J. C., SEBASTIAN D., LAZARO M. J., Synthesis and applications of carbon nanofibers: a review, Rev. Chem. Eng. 36, 493-511 (2020).
15. WANG K., WANG Y., WANG Y., HOSONO E., ZHOU H. S., Mesoporous carbon nanofibers for supercapacitor applications, J. Phys. Chem. C 113, 1093-1097 (2009).
16. P. RUVINSKYI, A. BONNEFONT, C. PHAM-HUU, E. R. SAVINOVA, Using ordered carbon nanomaterials for shedding light on the mechanism of the cathodic oxygen reduction reaction. Langmuir 27, 9018-9027 (2011).
17. J. K. CHINTHAGINJALA, J. H. BITTER, L. LEFFERTS, Thin layer of carbon nano-fibers (CNFs) as catalyst support for fast mass transfer in hydrogenation of nitrite, Appl. Catal. A: Gen. 383, 24-32 (2010).
18. LIU Y., LUO J., HELLEU C., BEHR M., BA H., ROMERO T., HÉBRAUD A., SCHLATTER G., ERSEN O., SU D. S., PHAM-HUU C., Hierarchical porous carbon fibers/carbon nanofibers composites from electrospinning/CVD processes as high effective surface area support platform. J. Mater. Chem. A, 5, 2151-2162 (2017).
19. E. FRECHA, J. REMON, D. TORRES, I. SUELVES, J. L. PINILLA, Design of highly active Ni catalysts supported on carbon nanofibers for the hydrolytic hydrogenation of cellobiose, Front. Chem. Volume 10 (2022). https://doi.org/10.3389/fchem.2022.976281
20. C. F. SANZ-NAVARRO, P. O. ASTRAND, D. CHEN, M. RONNING, A. C. T. VAN DUIN, T. JACOB, W. A. GODDARD, Molecular Dynamics Simulations of the Interactions between Platinum Clusters and Carbon Platelets. J. Phys. Chem. A 112, 1392-1402 (2008).
21. R. VIEIRA, C. PHAM-HUU, N. KELLER, M. J. LEDOUX, Iridium supported on carbon nanofibers/graphite felt composite catalyst for hydrazine decomposition. Chem. Commun. 9, 954-955 (2002).

22. F. SALMAN, C. PARK, R. T. K. BAKER, Hydrogenation of crotonaldehyde over graphite nanofiber supported nickel. Catal. Today 53, 385-394 (1999).
23. J. C. RUIZ-CORNEJO, J. E. VIVO-VILCHES, D. SEBASTIAN, M. V. MARTINEZ-HUERTA, M. J. LAZARO, Carbon nanofiber-supported tantalum oxides as durable catalyst for the oxygen evolution reaction in alkaline media, Ren. Energy 178, 307-317 (2021).
24. Y. MOTOYAMA, S. HOSOKAWA, Carbon nanofibers as supports for metal nanoparticles, Carbon 87, 463 (2015).
25. BA H., TRUONG-PHUOC L., LIU Y., DUONG-VIET C., NHUT J. M., NGUYEN-DINH L., GRANGER P., Pham-Huu C. Hierarchical carbon nanofibers/graphene composite containing nano-diamonds as metal-free catalyst for direct dehydrogenation of ethylbenzene. Carbon, 96, 1060-1069 (2016).
26. N. ABDULLAH, A. RINALDI, I. S. MUHAMMAD, S. B. ABD. HAMID, D. S. SU, R. SCHLÖGL, Catalytic Growth of Macroscopic Carbon Nanofibers Bodies with Activated Carbon, *AIP Conference Proceedings* 1136, 238–242 (2009). https://doi.org/10.1063/1.3160139
27. L. TRUONG-PHUOC, T. TRUONG-HUU, L. NGUYEN-DINH, W. BAAZIZ, T. ROMERO, D. EDOUARD, D. BEGIN, I. JANOWSKA, C. PHAM-HUU, Silicon carbide foam decorated with carbon nanofibers as catalytic stirrer in liquid-phase hydrogenation reactions. Appl. Catal. A: Gen. 469, 81-88 (2014).
28. YAOJIE CAO, PING LI**,** JINGHONG ZHOU**,** ZHIJUN SUI**,** XINGGUI ZHOU, WEIKANG YUAN, Pressure Drop of Structured Packing of Carbon Nanofiber Composite, Ind. Eng. Chem. Res. 49, 3944–3951 (2010).
29. A. RINALDI, N. ABDULLAH, M. ALI, A. FURCHE, S. B. ABD. HAMID, D. S. SU, R. SCHLÖGL, Controlling the yield and structure of carbon nanofibers grown on a nickel/activated carbon catalyst, Carbon 47, 3023-3033 (2009).
30. PHAM-HUU C., LEDOUX M.-J., Carbon nanomaterials with controlled macroscopic shapes as new catalytic materials, Topics Catal. 40, 49-63 (2006).
31. B. D. SOSNOWCHIK, L. LIN, O. ENGLANDER, Localized heating induced chemical vapor deposition for one-dimensional nanostructure synthesis. J. Appl. Phys. 107, 051101 (2010).
32. G. D. WEHINGER, Chem. Eng. Process. Intensif. 177, 108996 (2022).
33. K. AASBERG-PETERSEN, J. H. BAK HAUSEN, T. S. CHRISTENSEN, I. DUBKJAER, P. S. CHRISTENSEN, C. S. NIELSEN, S. E. L. W. MADSEN, J. R. ROSTRUP-NIELSEN, Appl. Catal. A Gen. 221, 379-387 (2001).
34. A. KIRSCHNING, L. KUPRACZ, J. HARTWIG, New synthesis opportunities in miniaturized flow reactors with inductive heating. Chem. Lett. 41, 562-570 (2012).
35. G. BENKOWSKY, Induktionserwärmung: Härten, Glühen, Schmelzen, Löten, Schweißen (Induction heating: hardening, annealing, melting, soldering and bracing, welding) 5th ed., Verlag Technik, Berlin, 1990, p. 12.
36. B. D. SOSNOWCHIK, L. LIN, Rapid synthesis of carbon nanotubes via inductive heating. Appl. Phys. Lett. 89, 193112 (2006).
37. Z. LI, B. ZHAO, P. LIU, B. ZHAO, D. CHEN, Y. ZHANG, Synthesis of high-quality single-walled carbon nanotubes by high-frequency-induction heating. Physica E 40, 452-456 (2008).
38. R. PINER, H. LI, X. KONG, L. TAO, I. N. KHOLMANOV, H. JI, W. H. LEE, J. W. SUK, J. YE, Y. HAO, S. CHEN, C. W. MAGNUSON, A. F. ISMACH, D. AKINWANDE, R. S. RUOFF, Graphene Synthesis *via* Magnetic Inductive Heating of Copper Substrates. ACS Nano 7, 7495–7499 (2013).
39. C. WU, F. LI, W. CHEN, C. P. VEERAMALAI, P. C. OOI, T. GUO, Electromagnetic induction heating for single crystal graphene growth: morphology control by rapid heating and quenching. Sci. Rep. 5, 9034, DOI: 10.1038/srep09034 (2015).
40. D. LUPU, A. R. BIRIS, A. JIANU, C. BUNESCU, E. BURKEL, E. INDREA, G. MIHAILESCU, S. PRUNEANU, L. OLENIC, I. MISAN, Carbon nanostructures produced by CCVD with induction heating. Carbon 42, 503-507 (2004).

41. Z. LI, B. ZHAO, P. LIU, B. ZHAO, D. CHEN, Y. ZHANG, Synthesis of high-quality single-walled carbon nanotubes by high-frequency-induction heating. Physica E 40, 452-456 (2008).
42. M. G. VINUM, M. R. ALMIND, J. S. ENGBAEK, S. B. VENDELBO, M. F. HANSEN, C. FRANDSEN, J. BENDIX, P. M. MORTENSEN, Dual function cobalt-nickel nanoparticles tailored for high-temperature induction-heated steam methane reforming. Angew. Chem. Int. Ed.
DOI: 10.1002/anie.201804832 (2018).
43. P. D. MULEY, C. HENKEL, K. K. ABDOLLAHI, D. BOLDOR, Pyrolysis and Catalytic Upgrading of Pinewood Sawdust Using an Induction Heating Reactor. Ener. Fuel 29, 7375−7385 (2015).
44. A. BORDET, L.-M. LACROIX, P.-F. FAZZINI, J. CARREY, K. SOULANTICA, B. CHAUDRET. Magnetically Induced Continuous CO_2 Hydrogenation Using Composite Iron Carbide Nanoparticles of Exceptionally High Heating Power. Angew. Chem. Int. Ed. 128, 1-6 (2016).
45. Y. LIU, P. GAO, N. CHERKASOV, E. V. REBROV, Direct amide synthesis over core-shell TiO_2@$NiFe_2O_4$ catalyst in a continuous flow radiofrequency-heated reactor. RSC Adv. 6, 100997-101007 (2016).
46. T. K. HOULDING, E. V. REBROV, Application of alternative energy forms in catalytic reactor engineering. Green Process Synth. 1, 19-31 (2012).
47. MARIN I. M., DE MASI D., LACROIX L.-M., FAZZINI P.-F., VAN LEEUWEN P. W. N.M., ASENSIO J.M., CHAUDRET B, Hydrodeoxygenation and hydrogenolysis of biomass-based materials using FeNi catalysts and magnetic induction. Green Chemistry 23, 2025, 2021.
48. GARCIA-AGUILAR, J., FERNANDEZ-GARCIA, J., REBROV, E. V., LEES, M. R., GAO, P., CAZORLA-AMOROSA, D., BERENGUER-MURCIA, A., Magnetic Zeolites: Novel Nanoreactors Through Radiofrequency Heating. *Chem. Commun.* **2017**, *53*, 4262-4265.
49. W. WANG, Z. XU, C. DUONG-VIET, G. TUCI, L. NGUYEN-DINH, G. GIAMBASTIANI, J.-M. NHUT, C., Pham-Huu. CO_2 methanation under discontinuous operation mode on nickel-decorated graphite felt with inductive heating. Catal. Today (2020).
50. W. WANG, C. DUONG-VIET, G. TUCI, J.-M. NHUT, Y. LIU, C. PHAM-HUU, Inductive heating: an enabling technology for the heat management in catalytic processes. ACS Catal. 9, 7921-7935 (2019).
51. F. VARSANO, M. BELLUSCI, A. LA BARBERA, M. PETRECCA, M. ALBINO, C. SANGREGORIO, Dry reforming of methane powered by magnetic induction. Int. J. Hyd. Energ. 44, 21037-21044 (2019).
52. WU L., MA H., YAN Z., XU Q., LI Z., Improving catalyst performance of Ni-CaO-C to enhance H_2 production from biomass steam gasification through induction heating technology, Energy Conv. Manag. 270, 1116242 (2022).
53. M. H. NGUYEN, M. C. PHAN, S. LIU, C. PHAM-HUU, L. NGUYEN-DINH, Radio-frequency induction heating powered low-temperature catalytic CO_2 conversion via bi-reforming of methane, Chem. Eng. J. 430, 132934 (2022).
54. B. D. SOSNOWCHIK, Y.-H. HA, L. LUO, L. LIN, Rapid, localized synthesis of titanium-based nanoswords on MEMS. 21st IEEE Micro Electro Mechanical Systems Conference (IEEE, Tucson, AZ, USA, 2008) 693 (2008).
55. B. D. SOSNOWCHIK, L. LIN, Rapid synthesis of carbon nanotubes by bulk and localized inductive heating. 20th IEEE Micro Electro Mechanical Systems Conference (IEEE, Kobe, Japan, 2007) 835 (2007).
56. YU Z., Effect of support and reactant on the yield and structure of carbon growth by chemical vapour deposition, J. Phys. Chem. B 109, 6096-6102 (2005).
57. ANDERSON P. E., RODRIGUEZ N. M., Growth of graphite nanofibers from the decomposition of CO/H_2 over silica-promoted iron-nickel particles, J. Mater. Res. 14, 2912-2921 (1999).
58. C. PHAM-HUU, R. VIEIRA, B. LOUIS, A. CARVALHO, J. AMADOU, T. DINTZER, M. J. LEDOUX, About the octopus-like growth mechanism of the carbon nanofibers over graphite supported nickel catalyst. J. Catal. 240, 194-202 (2006).

59. X. ZHANG, Y. LIU, X. MA, X. LIU, R. ZHANG, Y. WANG, Metal-support interaction of carbon-based electrocatalysts for oxygen evolution reaction, Nanoenergy Adv. 3, 48-72 (2023).
60. W. CHENG, P. YUAN, Z. LV, Y. GUO, Y. QIAN, X. XUE, X. LIU, W. BAI, K. WANG, Q. XU, J ZHANG, Boosting defective carbon by anchoring well-defined atomically dispersed metal-N_4 sites for ORR, OER and Zn-air batteries, Appl. Catal. B: Env. 260, 118198 (2020).
61. Q. ZHANG, Y. MA, J. MA, C. MENG, S. LUO, Y. LIU, Pd/oCNT monolith catalysts for continuous-flow selective hydrogenation of cinnamdehyde, ACS Appl. Nano Mater. 6, 8868-8879 (2023).
62. R. VIEIRA, M. J. LEDOUX, C. PHAM-HUU, Synthesis and characterization of carbon nanofibers with macroscopic shaping formed by catalytic decomposition of C_2H_6/H_2 over nickel catalyst. Appl. Catal. A 274, 1-8 (2004).
63. W. WANG, C. DUONG-VIET, L. TRUONG-PHUOC, J.-M. NHUT, L. VIDAL, C. PHAM-HUU, Activated carbon supported nickel catalyst for selective CO_2 hydrogenation to synthetic methane under contactless induction heating, Catal. Today 418, 114073 (2023).
64. M. MUNOZ, J. NIETO-SANDOVAL, E. SERRANO, Z. M. DE PEDRO, J. A. CASAS. CWPO intensification by induction heating using magnetite as catalyst, J. Env. Chem. Eng. 8, 104085 (2020).
65. S.-H. LIN, W. HETABA, B. CHAUDRET, W. LEITNER, A. BORDET, Copper-decorated iron carbide nanoparticles heated by magnetic induction as adaptative multifunctional catalysts for the selective hydrodeoxygantion of aldehydes, Adv. Energ. Mater. 12, 2201783 (2022).
66. W. WANG, C. DUONG-VIET, L. TRUONG-PHUOC, T. TRUONG-HUU, H. M. NGUYEN, L. NGUYEN-DINH, Y. LIU, C. PHAM-HUU. Improving catalytic performance via induction heating: selective oxidation of H_2S on a nitrogen-doped carbon catalyst as a model reaction, New J. Chem. 47, 1105-1116 (2023).
67. Q. LIANG, L. Z. GAO, Q. LI, S. H. TANG, B. C. LIU, Z. L. YU, Carbon nanotube growth on Ni-particles prepared in situ by reduction of La NiO_4, Carbon 39, 897 (2001).
68. S. SATO, A. KAWABATE, M. NIHEI, Y. AWANO, Growth of diameter-controlled carbon nanotubes using monodisperse nickel nanoparticles obtained with a differential mobility analyzer, Chem. Phys. Lett. 382, 361 (2003).
69. I. JULIAN, H. RAMIREZ, J. L. HUESO, R. MALLADA, J. SANTAMARIA, Non-oxidative methane conversion in microwave-assisted structured reactors, Chem. Eng. J. 377 (2019) 119764.
70. A. J. PAGE, Y. OHTA, S. IRLE, K. MOROKUMA. Acc. Chem. Res. 43, 1375-1385 (2010).
71. S. PORRO, S. MUSSO, M. VINANTE, L. VANZETTI, M. ANDERLE, F. TROTTA, A. TAGLIAFERNO, Purification of carbon nanotubes growth by thermal CVD, Phys. E: Low-dimensional Sys. Nanostruc. 37, 58-61 (2007).
72. D. WEI, Y. LIU, L. CAO, L. FU, X. LI, Y. WANG, G. YU, A magnetism-assisted chemical vapor deposition method to produce branched on iron-encapsulated carbon nanotubes, J. Am. Chem. Soc. 129, 7364-7368 (2007).
73. L. M. HOYOS-PALACIO, A. G. GARCIA, J. F. PEREZ-ROBLEO, J. GONZALEZ, H. V. MARTINEZ-TEJADA, Catalytic effect of Fe, Ni, Co and Mo on the CNTs production, IOP Conf. Series: Mater. Sci. Eng. 59, 012005 (2014)

Manuscript received: 20.06.2023